Applied Catalysis A: General 348 (2008) 173–182

Contents lists available at ScienceDirect

Applied Catalysis A: General

journal homepage: www.elsevier.com/locate/apcata

Influence of hydrothermal aging on the catalytic activity of sulfated zirconia

Mariana Busto [a], Kiyoyuki Shimizu [b], Carlos R. Vera [a,*], Javier M. Grau [a], Carlos L. Pieck [a], Miguel A. D'Amato [a], M.T. Causa [c], M. Tovar [c]

[a] Instituto de Investigaciones en Catálisis y Petroquímica -INCAPE- (FIQ-UNL, CONICET), Santiago del Estero 2654, 3000 Santa Fe, Argentina
[b] Council for Science and Technology Policy, Cabinet Office (AIST-MITI), 3-1-1 Kasumigaseki, Chiyoda-ku, Tokyo 100-8970, Japan
[c] Centro Atómico Bariloche, Comisión Nacional de Energía Atómica, Av. Ezequiel Bustillo 9500, 8400 San Carlos de Bariloche, Argentina

ARTICLE INFO

Article history:
Received 29 February 2008
Received in revised form 18 June 2008
Accepted 21 June 2008
Available online 1 July 2008

Keywords:
Reflux aging
Sulfated zirconia
n-Butane isomerization
n-Octane isomerization-cracking

ABSTRACT

The use of reflux aged zirconia gel in the synthesis of sulfated zirconia catalysts for isomerization of short paraffins and isomerization-cracking of long paraffins was assessed. It was found that reflux aging greatly improved zirconia textural properties. The growth of the monoclinic phase was greatly suppressed and the initial area and sintering resistance were increased. The specific surface area of reflux aged material with no sulfate was almost 75 $m^2 g^{-1}$ after calcination at 800 °C. Sulfate promotion of aged materials further increased the tetragonal/monoclinic ratio and the area of sulfated catalysts was 220 $m^2 g^{-1}$ after calcination at 600 °C.

Impregnation of reflux aged materials with sulfate produced materials which had very low activity in isomerization of *n*-butane. The effect of aging was explained in terms of a dissolution-precipitation process that eliminated specific sites of the gel that were responsible for much of the activity of the final catalyst. In the case of the hydroisomerization-cracking of long paraffins the effect was less deletereous partly due to the higher reactivity of this feedstock.

1. Introduction

Oxoanion promoted zirconia catalysts have outstanding properties of conversion of short paraffins at low temperature with high selectivity to branched isomers. Currently Pt/SO_4^{2-}–ZrO_2 and Pt/WO_3–ZrO_2 are the basis of commercial C_5–C_6 virgin naphtha isomerization process like the Par-Isom (UOP) and EMICT (Exxon-Mobil) ones. New formulations are constantly tried to improve their activity and selectivity for new applications [1,2]. As for any other catalyst the improvement of the textural properties of oxoanion promoted zirconia catalysts is an important issue. It is known that common oxoanions like sulfate and tungstate produce a textural promotion and the catalysts have a preferential presence of the tetragonal structure, while the sintering resistance and the total area are higher than those of pure zirconia after calcination at high temperatures [3–5]. This is true only when the calcination does not produce the decomposition of the adsorbed oxoanion layer. At temperatures higher than 650–700 °C sulfate decomposes and the zirconia support sinters rapidly into the monoclinic form [6]. Sintering decreases the available surface area to negligible values in this process. At temperatures lower than those of decomposition the temperature needed for the obtention of maximum activity is also sufficiently high to decrease the area to small values. For SO_4^{2-}–ZrO_2 (SZ) calcination at 600–650 °C yields catalysts with 100–120 $m^2 g^{-1}$ and in the case of WO_3–ZrO_2 (WZ) calcination at 800 °C decreases the final area to 20–60 $m^2 g^{-1}$. A higher specific surface area translates into a higher activity per unit volume and reactor sizes can be decreased in new process designs or the production can be increased in reactor revamps.

Another textural property that can be improved for the benefit of some processes is the mesoporosity. In the case of sulfated zirconia the pore structure spans both the micropore and mesopore range. Though the microporosity contributes to a great extent to the total available surface this area sometimes cannot be reached due to mass transfer limitations. This is the case when bulky molecules are involved in the reaction. Moreover if micropores are in the way of a wider pore inner volume the access to other wider pores is also restricted.

Stabilization of the tetragonal phase seems to be another important issue because oxoanion promoted monoclinic zirconia is catalytically less active for many acid-catalyzed reactions, like *n*-butane isomerization and dehydration of 2 octanol [4,7]. Completely amorphous catalysts are also inactive. Additional

* Corresponding author.
E-mail address: cvera@fiq.unl.edu.ar (C.R. Vera).

0926-860X/$ – see front matter © 2008 Elsevier B.V. All rights reserved.
doi:10.1016/j.apcata.2008.06.029

textural improvements in oxoanion promoted zirconia catalysts could be obtained by adopting different synthesis methods for the zirconia gel. Some encouraging results have been found for tungsten-zirconia and sulfated zirconia obtained by the promotion of zirconia aerogels. These aerogels have a very high initial surface that is produced by supercritical drying [8–10]. Mesoporous zirconias produced by cogellation with molecular templates have also been produced [11,12] but their structure is brittle and collapses during calcination at relatively low temperatures. Additional stabilization of the gel pore structure could also be achieved by incorporating surface or bulk dopants into sulfate or tungsten-zirconia. In many cases when a marked enhancement of the sintering resistance or the microporosity are obtained this is in detriment of the catalytic activity, as it happens with silica addition [13–15]. New methods of improving the textural properties should be found that do not affect the catalytic properties of oxoanion promoted zirconia catalysts [16,17]. These should produce a greater noticeable increase in surface area, sintering resistance and tetragonal/monoclinic ratio beyond that produced by the surface oxoanion promoter itself. In this work we report our results on the use of hydrothermally aged zirconia for the preparation of SO_4^{2-}-ZrO_2 catalysts. The influence of reflux aging on textural properties and catalytic activity for isomerization of *n*-butane and hydroisomerization-cracking of *n*-octane were assessed.

Hydrothermal aging is a rather old technique for the improvement of the texture of the gel of precipitated hydroxides. Aging is thought to be related to a process of simultaneous dissolution and precipitation which favors the growth of "neck structures" in the gel network. During the process the support dissolves from regions of positive curvature and redeposits at regions of negative curvature reinforcing the hydrogel network [18]. This lattice refining removes brittle structures and a more homogeneous network is produced. SEM images of materials aged in aqueous medium or in molten salt baths reveal a "cheese" like structure [19]. Our study is concentrated on zirconia gels reflux aged at strong basic pH values because in this condition the stabilization of the tetragonal active phase seems to be complete and sintering resistance is very high [20].

2. Experimental

2.1. Catalyst preparation

2.1.1. Zirconia gels

Reflux aged $Zr(OH)_4$ was prepared from $ZrOCl_2{\cdot}8H_2O$ (Strem Chem., 99.9985%). A solution of the salt (0.4 M in Zr^{4+}) was allowed to drip over an ammonia solution (5 M NH_4OH, with a volume of 2 times that of the dripping solution) and under constant stirring. The freshly precipitated gel was gently refluxed for 120 h at about 100 °C in a rotating Büchi evaporator heated by an oil bath. Successive cycles of decantation-washing (15–20) were then performed. They were considered enough for the elimination of the ammonium and chloride ions. Then the gel was filtered and dried at 110 °C overnight (sample Z^{AG}). For another batch of zirconia reflux aging was eliminated and the gel was only kept overnight at room temperature. After washing, filtering and drying, a reference non-aged batch of zirconia was obtained (sample Z). The portion of these solids (Z^{AG} and Z) were fired at three different temperatures (500, 600 and 800 °C) in static air in a muffle oven.

2.1.2. Sulfated catalysts

They were prepared by wet impregnation. The dried samples (Z, Z^{AG}, dried at 110 °C) were dipped in a 1N H_2SO_4 solution for 2 h (10 ml g^{-1}). After sulfation all catalysts (SZ and SZ^{AG}) were calcined at 500 °C, 600 °C and 800 °C for 3 h in static air in a muffle oven.

2.1.3. Pt/SO_4^{2-}–ZrO_2 catalysts

The sulfated zirconia gels, either aged or non-aged, were impregnated with an aqueous solution of chloroplatinic acid (Strem Chem., 99.9%) using the incipient wetness technique (addition of a volume of solution equal to the catalyst pore volume). The time of impregnation was 6 h. The samples were then dried at 110° overnight and calcined at 500 °C in flowing air for 2 h. The volume and concentration of the impregnating solution were adjusted to get a 1% Pt in the final catalyst (Pt/SZ and Pt/SZ^{AG}).

2.2. Catalyst characterization

2.2.1. Sulfur content

It was measured in a LECO CS444 carbon and sulfur analyzer using direct combustion and infrared detection.

2.2.2. Platinum content

It was determined by inductively coupled plasma-atomic emission spectroscopy (ICP-AES) after digesting the samples.

2.2.3. X-ray diffraction measurements (XRD)

The XRD measurements were performed in a Shimadzu XD-1 diffractometer with Cu Kα radiation filtered with Ni. Spectra were recorded in the 20–65° 2Θ range and scanned at a rate of 1.2° min^{-1}.

2.2.4. Textural properties

They were measured in a Belsorp 28 SA nitrogen adsorption apparatus. The specific surface area (Sg) was measured by the BET method and the pore distribution by the D–H (Dollimore and Heal) method.

2.2.5. Raman

Laser Raman spectra were recorded in a Spectramax equipment having a NEC Ar ion laser (514.5 nm) and operating with a laser power of 40–50 mW. The detector was a CCD Yobin Yvon HR320 with a Hg baseline of 1122.74 cm^{-1} and a slit of 25 μm.

2.2.6. Temperature-programmed reduction (TPR)

Tests were performed in an Ohkura TP2002 S apparatus equipped with a thermal conductivity detector. The samples were heated from room temperature to 750 °C at 10 °C min^{-1} in a reducing gas stream (5% H_2 in Ar, of 45 ml min^{-1}).

2.2.7. Temperature-programmed oxidation (TPO)

Tests were carried out in an apparatus with intermediate methanation and with detection by flame ionization (FID). The catalyst sample was heated from room temperature to 700 °C at 12 °C min^{-1} in an oxidizing gas stream (30 ml min^{-1}, 2.3% O_2 in N_2).

2.2.8. Temperature-programmed desorption (TPD) of probe molecules

Acidity was measured by adsorption of pyridine. The adsorption was performed in a glass equipment. The adsorbed amount was assessed by light absorption in the infrared region (1400–1600 cm^{-1} range). The measurements were performed in a Nicolet Avatar 360 FT-IR spectrometer. Self supported circular wafers (2 cm diameter, 50 mg) of the catalysts were used and they were vacuum treated in a cell with NaCl windows. Residual pressure was less than 1 mTorr. Additional experiments of temperature programmed desorption of pyridine were also performed. 200 mg of the catalyst were first immersed in a closed vial

containing pure pyridine (Merck, 99.9%) for 4 h. Then the catalyst was taken out from the vial and excess pyridine was removed by evaporation at room temperature under a fume hood. The sample was then charged to a quartz micro reactor and a constant nitrogen flow (40 $cm^3\ min^{-1}$) was established. Weakly adsorbed pyridine was first desorbed in a first stage of stabilization by heating the sample at 110 °C for 2 h. The temperature of the oven was then raised to 600 °C at a heating rate of 10 °C min^{-1}. The reactor outlet was directly connected to a flame ionization detector to measure the desorption rate of pyridine.

2.2.9. Electron spin resonance

In order to detect the presence of Zr^{3+}, we performed Electron Spin Resonance (ESR) experiments using a Bruker ESP300 spectrometer operating at X-band (microwave frequency $\nu = 9.4$ GHz) with applied magnetic fields up to 2 T. All the experiments were performed at room temperature.

2.2.10. Infrared spectroscopy (FT-IR)

Infrared spectra were obtained using a Shimadzu 8101 M spectrometer. Samples were prepared in the form of pressed wafers. All spectra involved the accumulation of 64 scans at 8 cm^{-1} resolution. The sample was dried for 2 h at 400 °C and a vacuum of 10^{-5} Torr. Then NO was adsorbed at room temperature and at a pressure of 3 Torr.

2.3. Catalyst tests

2.3.1. Isomerization n-butane

Before the reaction all the samples were activated in a flow of air at 620 °C. Then the temperature was lowered to the reaction temperature (300–350 °C) and the gas flow was switched to the carrier and stabilized for 30 min before beginning the reaction. Pure *n*-C_4 (99.99%) was used. Each pulse had a volume of 0.32 ml which was sent to a quartz microreactor (20 cm long, 4 mm internal diameter) by the carrier gas (10 ml min^{-1}) and a sampling valve. Samples of 150 mg of the catalysts were used all throughout the experiments. The pulses were collected at the exhaust of the reactor with a gas tight ampoule and analyzed off-line in a gas chromatograph. The carrier gas used was nitrogen and the temperature of reaction was 300 °C.

2.3.2. Isomerization-cracking of n-octane

An amount of catalyst in order to keep a constant mass of 0.5 g of sulfated zirconia in each test was loaded in a plug-flow reactor connected to gas chromatograph. Reaction conditions were: 300 °C, 1.5 MPa, WHSV = 4 and H_2/*n*-C_8 = 6 (molar ratio), total time-on-stream = 10 h. Before the reaction the catalysts were heated from room temperature to 300 °C in hydrogen (2.3 °C min^{-1} heating rate) and kept for 1 h at 300 °C and 1.5 MPa. The *n*-C_8 feedstock was Carlo Erba pro analysis and the hydrogen was supplied by AGA.

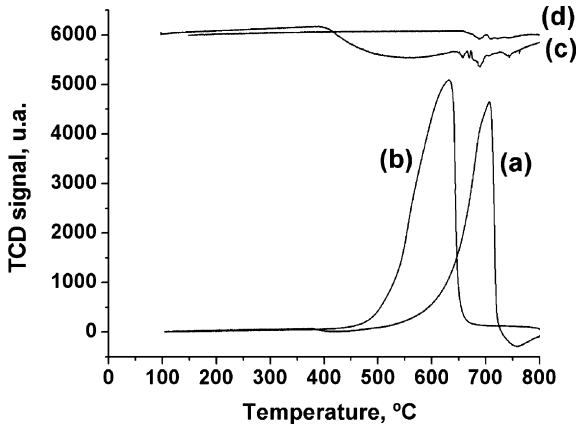

Fig. 1. TPR and TPO of SZ catalysts. (a) TPR of SZ, (b) TPR of SZ^{AG}, (c) TPO of SZ^{AG} and (d) TPO of SZ.

3. Results and discussion

3.1. Chemical composition, textural properties

Table 1 shows the results of the chemical analysis of the reflux aged materials after being calcined at 110 and 600 °C. Reflux aged materials incorporated a big amount of nitrogen species, which might have been present in the form of NH_4^+ cations. These cations must have been preferentially adsorbed on the surface because inclusion in the lattice is rather sterically hindered (ionic radii of species: O^{2-} = 0.124 nm, Zr^{4+} = 0.098 nm, OH^- = 0.118 nm, NH^{4+} = 0.163 nm [21]). The nitrogen content was drastically reduced after calcination at 600 °C and practically no nitrogen was present on the solid. With respect to the sulfur content there is a clear difference between the bulk and surface contents of aged and non-aged sulfated catalysts. When the bulk content is inspected, SZ^{AG} (1.58% S) has a higher content than SZ (0.87% S). In contrast when the surface sulfur density is compared, SZ (2.3 S nm^{-2}) has a higher density than SZ^{AG} (1.35 S nm^{-2}). The latter is somewhat lower than the average half-monolayer value usually found in common sulfated zirconia catalysts (2 S nm^{-2}) [22,23] or the monolayer value found in some cases [24]. In the case of the non-aged sulfated zirconia catalyst, SZ, the surface density was closer to the half-monolayer value, 2.3 S nm^{-2}. It can be seen that the capacity of retaining sulfur after calcination at 600 °C is reduced by the aging procedure.

TPO and TPR experiments were performed both on aged and non-aged sulfated materials calcined at 600 °C. The results can be seen in Fig. 1. The total area of the trace of the TCD signal is approximately proportional to the sulfur content of each sample. It can be seen that though the areas are fairly similar in the TPR traces, the ranges of decomposition are different. The sulfur on aged materials is lost at lower temperatures. This would indicate a

Table 1
Chemical composition and average textural properties

Samples	Nitrogen (%)	Sulfur (%)	$I^M/I^{T(1)}$	Surface area ($m^2\ g^{-1}$)	BET constant	Surface content *S* (groups nm^{-2})
Z, dried at 110 °C	0.58	–	–	254	2087.1	–
Z, calcined at 600 °C	0.00	–	0.67	45.0	–	–
Z, calcined at 800 °C	0.00	–	∞	5.7	–	–
Z^{AG}, dried at 110° C	2.6	–	–	416.37	422.55	–
Z^{AG}, calcined 600 °C	0.004	–	0.00	96.85	261.46	–
Z^{AG}, calcined at 800 °C	0.001	–	0.11	73.52	94.95	–
SZ^{AG}, calcined at 600 °C	0.001	1.58	0.00	220.16	–	1.35
SZ, calcined at 600 °C	0.00	0.87	0.17	71.49	–	2.3

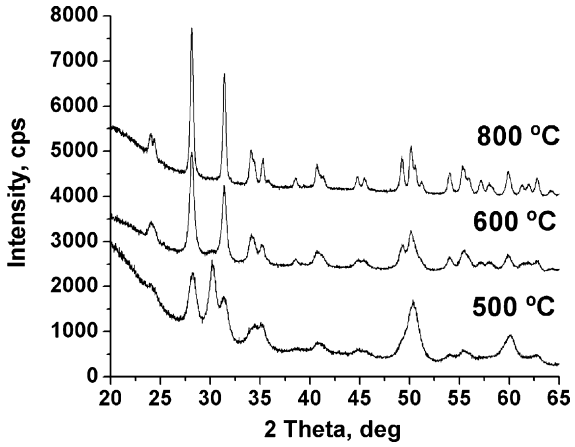

Fig. 2. XRD spectra of non-aged zirconia (Z) calcined at different temperatures.

higher reducibility of the sulfur species on aged zirconia due to a lower interaction with the support. In the case of the TPO traces the interpretation of the results is less clear, due to a broad envelope that occurs in the case of the aged sample and that overlaps with the high temperature peaks. It must be recalled that SZ^{AG} in this test had already been calcined and the sulfur content was already stabilized by thermal decomposition of labile S. The high temperature peaks in this sample (SZ^{AG}) start at about 600 °C (earlier than SZ). The presence of the envelope at lower temperatures would also indicate that sulfate groups are more labile on SZ^{AG}.

3.1.1. Crystal structure

Zirconia exhibits three well established forms, the monoclinic (baddeleyite) (M), tetragonal (T) and cubic (C) phases. The monoclinic phase is stable up to 1170 °C and then transforms into the tetragonal phase which is stable up to 2370 °C. At higher temperatures the cubic phase is the stable phase. Both the cubic and the tetragonal phase are fluoritic and cannot be "quenched". They can be however obtained under metastable conditions at lower temperatures. A clear distinction between the cubic and tetragonal phases is difficult by XRD methods because they are very similar and the small differences are not clear in samples of low crystallinity. The tetragonal phase peaks are located at $2\theta = 29.8°$ (main), 34.0°, 34.8°, 49.4°, 50.1° and 59.4°. The peaks of the cubic phase are located at $2\theta = 30.5°$ (main), 35.2°, 50.6° and 60.3°. The main peaks of the monoclinic phase are located at 28.2° and 31.5°.

Spectra of the non-aged (Z) zirconia gels calcined at different temperatures can be seen in Fig. 2. At low temperatures of calcination (500 °C) the structure was a mixture of the tetragonal and monoclinic phases. At temperatures equal to or higher than 600 °C the tetragonal structure disappeared and only peaks corresponding to the M phase could be found. Spectra of reflux aged (Z^{AG}) and non-aged sulfated zirconia (SZ) can be found in Fig. 3. It can be seen that aging suppresses the growth of the monoclinic phase of zirconia while stabilizing a fluoritic phase. From the XRD data it cannot be distinguished clearly if this fluoritic structure is tetragonal or cubic. Inspection of the Raman spectrum of Z^{AG} calcined at 800 °C (Fig. 4) confirms that the structure is tetragonal. Four bands can be seen, at 266, 315, 459, 600 and 644 cm^{-1}. Cubic zirconia is known to have only a broad band at 259 cm^{-1} [25,26]. Tetragonal zirconia is known to have bands at 263, 472, 608 and 640 cm^{-1} [27].

Fig. 3 shows that calcination at 600–800 °C produces a great growth of the monoclinic phase in non-aged materials. In the modified materials stabilization of the T phase by aging or sulfation was similar at 600 °C. At higher temperatures T phase stabilization by aging was more effective than that produced by sulfation since non-aged sulfated materials are irreversibly converted to the monoclinic phase upon removal of the surface sulfates [6]. SZ calcined at 800 °C was mainly monoclinic and sulfate decomposition was detected in the TPO experiments at 650–750 °C. Loss of the stabilizing anion triggered the T → M transition in this case. Meanwhile aged tetragonal materials, with or without sulfate, were scarcely affected in their structure.

Values of the monoclinic to tetragonal ratio (I^M/I^T, ratio of the intensity of the main peaks of the monoclinic (M) and tetragonal (T) phases at $2\theta = 28.2$ and 30°) are included in Table 1. They ranged from 0.0 for SZ^{AG} calcined at 600 °C to ∞ in the case of Z calcined at 800 °C. For SZ^{AG} tetragonality was the highest and the M phase was completely absent in the sample calcined at 600 °C. In comparison with non-aged, non-sulfated zirconia (Fig. 2) crystallinity of sulfated and/or aged materials, as estimated by inspection of the intensity and width of the XRD peak, was low. In the case of the sulfate materials this is due to the disturbing effect of sulfate, which is known to shift the crystallization temperature and slow down the crystal growth [4]. Aging also hampered the crystal

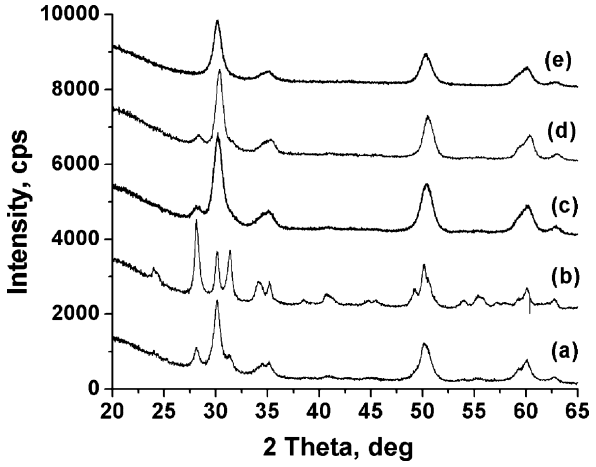

Fig. 3. XRD spectra of reflux aged and sulfated samples calcined at different temperatures. (a) Sulfated zirconia non-aged (SZ), calcined at 600 °C; (b) sulfated zirconia non-aged (SZ), calcined at 800 °C; (c) reflux aged zirconia (Z^{AG}) calcined at 600 °C; (d) reflux aged zirconia (Z^{AG}) calcined at 800 °C; (e) reflux aged sulfated zirconia (SZ^{AG}), calcined at 600 °C.

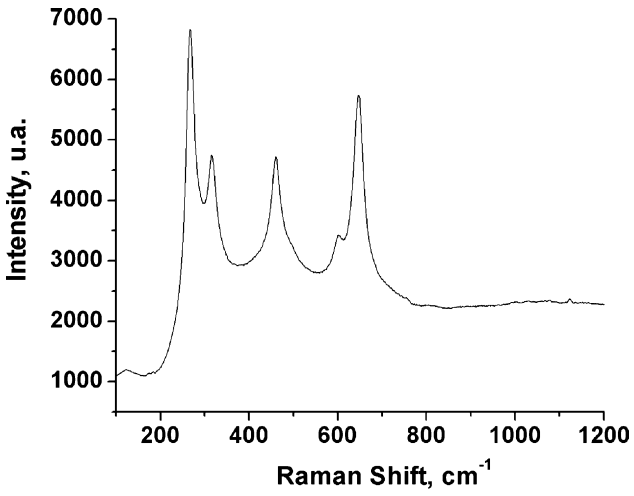

Fig. 4. Raman spectra of reflux aged zirconia (Z^{AG}).

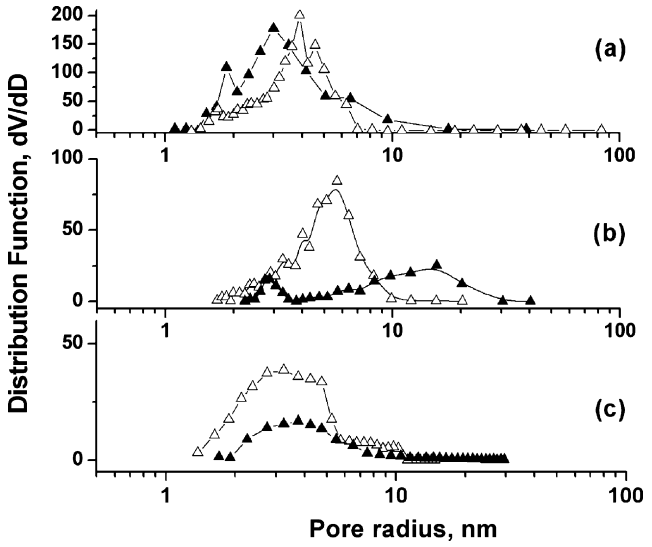

Fig. 5. Pore size distribution of zirconia materials. (a) (▲) $Zr(OH)_4$, dried at 110 °C; (Δ) $Zr(OH)_4$ reflux aged for 120 h, dried at 110 °C; (b) (▲) Z calcined at 800 °C for 3 h (multiplied by 5), (Δ) Z^{AG}, calcined at 800 °C for 3 h; (c) (▲) SZ, calcined at 600 °C, (Δ) SZ^{AG} calcined at 600 °C.

growth. For SZ^{AG} crystallinity was the lowest. This result correlated with the specific surface area of this material, which was the highest.

3.1.2. Surface area, pore structure

The results of textural properties for the aged and non-aged zirconia supports and catalysts are listed in Table 1. Calcination of the non-aged, non-sulfated, dried gel (ZH), drastically reduced its area to negligible values and produced a growth of the monoclinic crystal phase. Reflux aged zirconia samples where more resistant to sintering and had almost 100 $m^2\ g^{-1}$ when calcined at 600 °C and more than 70 $m^2\ g^{-1}$ at 800 °C. After calcination at 600 °C the area of the aged material with no sulfate was even higher than the area of the calcined sulfated xerogel. The proportion of tetragonal phase was also higher. This indicates that the textural promotion produced by aging is much stronger than that produced by surface doping with sulfate. When sulfation and aging were combined, as in the SZ^{AG} catalyst, the sintering resistance was the highest. The high area of the SZ^{AG} sample calcined at 600 °C catalyst was remarkable (220 $m^2\ g^{-1}$). Reported data for sulfated zirconia gels fired at this temperature are always lower than 200 $m^2\ g^{-1}$, even for supercritically dried SZ aerogels [8].

Data for the pore distributions as measured by the D–H method applied to the desorption isotherm of nitrogen can be found in Fig. 5. When the Z and Z^{AG} samples dried at 110 °C are compared (Fig. 5a) we can see that both samples were mesoporous and that non-aged zirconia (Z) had a greater proportion of micropores. The maximum of the distribution was centered at 3.5–4.5 nm for Z^{AG}. Z had two maxima at 1.5–1.8 and 2.8 nm. Z^{AG} had practically no macropores greater than 10 nm while non-aged zirconia had macropores up to 40 nm. The aging treatment reduced the spread of the pore distribution of the zirconia gel and concentrated most pores at 3.5–4.5.

Fig. 5b contains the pore size distribution curves of the aged and non-aged gels calcined at 800 °C. After calcining at 800 °C the original Z^{AG} distribution became smaller and was shifted to 5–6 nm while still keeping a rather narrow profile. In the case of the *Z* sample the total pore volume collapsed and the distribution became wider, flat and centered at 12–20 nm. For this sample the process of pore growth was accompanied by a marked decrease in surface area due to the collapse of both the micro and mesopores. Micropores have a higher surface area per unit volume than mesopores and their loss has a higher impact on the final surface area. At 800 °C most of the area must be related to the external particle surface. In the case of the reflux aged zirconia the preservation of the area is related to the production of a sintering resistant mesoporous structure. The variation of the average pore radius for this structure was of only 1.5 nm.

Fig. 5c contains the pore size distribution data of the aged and non-aged, sulfated gels calcined at 600 °C. The effect of calcination can be approximately assessed by comparison with the curves of Fig. 5a since sulfation does not change the shape of these distributions very much (not shown). For the non-aged sulfated gel the effect of calcination is to shift the center of the pore size distribution from 3 to 4 nm and to decrease the total pore volume. The distribution becomes monomodal and the pores with radius lower than 2 nm are practically eliminated. In the case of the aged sulfated gel calcination does not produce a shift of the center of the distribution. The total pore volume is decrease but notably the pores smaller than 3 nm are less affected than the bigger ones.

A surface refining process produced by the dissolution-precipitation equilibrium under reflux conditions, could be approximately assessed by inspecting the value of the BET C constant for the sample before being aged (*Z*) and after the hydrothermal treatment (Z^{AG}) (Table 1). The constant is reduced by 5 times and accordingly the heat of adsorption is reduced by the same proportion. This indicates that many surface imperfections with high energy are eliminated and the average surface energy is decreased. Further reduction in the constant is brought by calcination.

Štefanić et al. [28] have reported that at temperatures between 90 and 120 °C either for HfO_2 or ZrO_2 hydrothermal crystallization proceeds via a dissolution-precipitation mechanism in the whole pH range. Dissolution refers to the entrance of cations into the solution and precipitation to the grafting of monomers or oligomers from the solution onto the particle surface. At a molecular level these processes correspond to hydrolysis and polycondensation reactions and temperature and pH are the primary variables involved. These variables also dictate the stability and the values of the rates of dissolution and precipitation of the solid phases involved [28]. The occurrence of dissolution-precipitation mechanism is usually accompanied by the growth of neck structures between particles [28].

Micropores have effective diameters between 0.3 and 2 nm. Mesopores diameters lie between 2 and 50 nm. An increase in the mesoporosity and a decrease of the microporosity upon hydrothermal aging of the zirconia gel is evident from the results of Fig. 5a. This is also the case for many other oxides hydrothermally aged. In the case of TiO_2 not only mesopores are favored but higher temperatures aging increase the average pore diameter accordingly [29]. Micropores transform into mesopores by dissolution of material from the walls. Adjacent micropores can also coalesce in the process if they are sufficiently nearby.

3.1.3. Acidity

The acidity of the sulfated and calcined samples was assessed by means of static pyridine adsorption and recording of the FTIR spectra of the adsorbate (Fig. 6) and by temperature programmed desorption of pyridine (Fig. 7). SZ^{AG} calcined at 600 °C had a high amount of acid sites (180 μmol g^{-1}) which were 69% of the Lewis type and 31% of the Brönsted type on average. The relative higher concentration of Lewis acid sites was due to the high calcination temperature that makes most Brönsted acid sites present on the hydrated surface at room temperature to transform into Lewis acid ones by dehydration. If we classify sites according to their pyridine

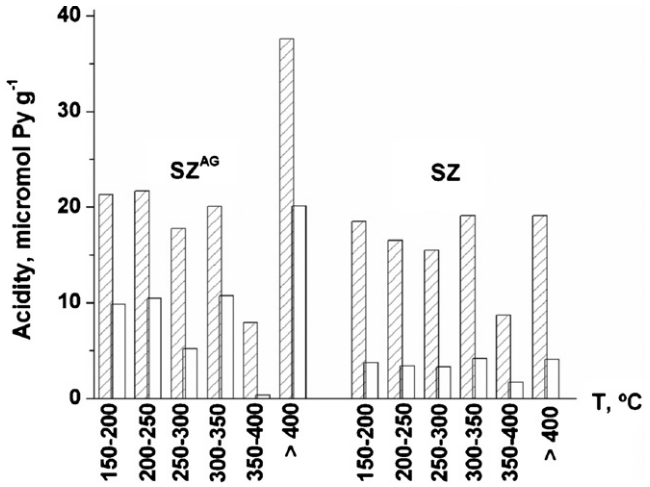

Fig. 6. Acidity as measured by FT-IR absorption of adsorbed pyridine. Shaded bars: Lewis. Blank bars: Brönsted.

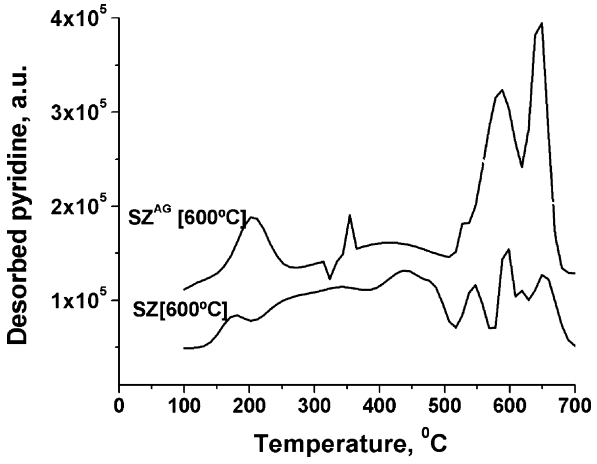

Fig. 7. Acidity as measured by temperature programmed desorption of adsorbed pyridine.

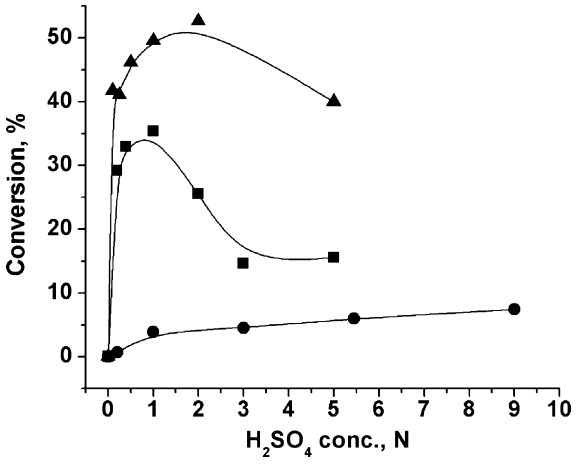

Fig. 8. Initial conversion of *n*-butane (first pulse) on sulfate-zirconia catalysts. (■) From non-aged zirconia [30]; (■) from non-aged zirconia (this work); (●) from aged zirconia.

desorption range in weak (<250 °C), mild (250–400 °C) and strong (>400 °C), we can see that in SZ^{AG} the amounts of weak and mild acid sites are similar and fairly superior to the amount of strong acid sites.

The acidity of non-aged SZ was 118 μmol g^{-1}. The population comprised 82% Lewis acid sites and 18% Brönsted ones. Strong acid sites desorbing at temperatures higher than 400 °C were 25 μmol g^{-1}. In SZ the amount of mild acid sites was bigger than that of weak acid sites and much bigger than that of strong acid sites. If we make a comparison between SZ^{AG} and SZ we can see that SZ^{AG} has a higher relative concentration of strong acid sites and a higher Brönsted/Lewis ratio. In order to confirm the results further acidity measurements were performed by temperature programmed desorption of pyridine. This technique probes both Lewis and Brönsted acid sites. The results can be inspected in Fig. 7. These results seem to confirm the FTIR results. The two TPD traces have peaks located in common positions. Weak acid sites desorb pyridine in a peak located at 180–200 °C. This peak is fairly big in SZ^{AG} and much smaller in SZ. A broad envelope between 250 and 500 would correspond to mild acid sites. This envelope is bigger for SZ. Three peaks located at 530–550 °C, 580 °C and 650 °C would correspond to strong acid sites of different acid strength. As it was the case with the FTIR data, SZ^{AG} had the highest concentration of total acid sites and of strong acid sites.

A comparison of the total acidity of both samples on a mass basis might be misleading because the total surface area of SZ^{AG} (220.16 m^2 g^{-1}) is much higher than of SZ (71.49 m^2 g^{-1}). If the acidity per unit area is calculated the relative order is changed: SZ^{AG} (0.82 μmol m^{-2}) < SZ (1.65 μmol m^{-2}). The higher acid surface density of SZ correlates with the higher sulfur surface density (SZ^{AG} = 1.35 S nm^{-2}, SZ = 2.3 S nm^{-2}).

3.1.4. Catalytic activity

The results of catalytic activity indicated that hydrothermal aging produced a deletereous effect on catalytic activity. Results corresponding to the initial conversion of sulfated materials can be found in Table 2. Non-aged sulfated zirconia had a higher activity than the reflux aged material. SZ^{AG} though it had the highest area (220 m^2 g^{-1} after calcination at 600 °C) had much lower activity than SZ.

Results of initial catalytic activity as a function of the concentration of the sulfuric acid impregnating solution are included in Fig. 8. Two experimental curves corresponding to the SZ and SZ^{AG} samples were plotted together with the data of D'Amato et al. [30]. The latter correspond to experiments with non-aged gels and have been included to confirm the activity pattern in the catalysts produced by sulfation of freshly precipitated, non-aged gels.

The plot of activity as a function of concentration of the sulfating solution for the aged sulfated gel (Fig. 8) is revealing.

Table 2
n-Butane reaction

Sample	1° pulse				5° pulse			
	Conv. rate	Sel. C_1–C_3	Sel. *i*-C_4	Sel. C_5	Conv. rate	Sel. C_1–C_3	Sel. *i*-C_4	Sel. C_5
SZ	1464.0	51.59	42.80	5.61	751.5	24.29	67.48	8.23
SZ^{AG}	114.5	22.98	69.45	7.56	67.86	13.22	76.28	10.6

Conversion rates (μmol g^{-1} min^{-1}) and selectivity values (%) of sulfated zirconia catalysts at the first and fifth pulse.

Common sulfate-zirconia produced by sulfation of non-aged gels always displayed a volcano shaped curve, as already reported by several researchers for *n*-butane isomerization [30,31] or other reactions. A volcano shaped plot was obtained in the case of SZ. No volcano shaped plot was found for reflux aged zirconia. The volcano curve can be divided into three regions of different behavior:

(1) *0–0.2N*: in this zone a steep increase of the catalytic activity occurs upon the treatment with relatively diluted solutions [30,31]. At 0.2N almost 80–90% of the maximum catalytic activity can be obtained. This zone has been attributed in early works on SZ to the deposition of sulfur species on defective surface sites, which would be selectively titrated [32]. In the particular cases of anionic vacancies the high affinity of SO_3 for them has been used to titrate their surface concentration [33]. In experiments of controlled sulfate deposition by incipient wetness Yori et al. [34] reported that for sulfated zirconia catalysts the first sites to be formed, which were less than 10% of the total sulfate groups, provided almost all the activity in *n*-butane isomerization. Morterra et al. [35] reported that sulfate groups on kinks, edges and other crystal imperfections were first to be sulfated, very stable upon calcination and a source of strong isolated Lewis acid sites.
(2) *0.2–2.0N*: in this range the activity increases slightly and reaches the maximum value. In this zone the use of impregnating solutions with progressively higher sulfuric acid concentrations succeeds in getting higher final sulfate contents in the sulfated gel [30] but the final sulfate content after calcination at 550–650 °C is never higher than the stable value of half a monolayer (2 S nm^{-2}) and the rest is decomposed [22,23]. Sulfate groups would be attached on regular zirconia planes and the textural promotion reaches its best results; samples in this range show the highest specific surface area values.
(3) *2.0–10.0N*: this is a zone of net decreasing catalytic activity. A plateau has already been reached in the final density of sulfur sites and the only effect taking place is that of destruction of the structure of the gel by acid leaching. The reported final specific surface area values are much lower than those of zone (2).

In the case of the reflux aged material no volcano plot could be seen and only a slight increase of the *n*-butane conversion with H_2SO_4 concentration. The sample sulfated with H_2SO_4 1N and calcined at 600 °C had an area of 220 $m^2\ g^{-1}$, a sulfur content of 1.58% (1.35 S nm^{-2}) and an initial conversion of 3.86%. The sample sulfated with H_2SO_4 9.0N had an area of 60 $m^2\ g^{-1}$, a sulfur content of 0.62% (1.91 S nm^{-2}) and an initial conversion of 7.43%. This trend of increasing activity with decreasing values of surface area does not match previous results of other authors working with non-aged sulfated zirconia. As discussed in the previous paragraph normally in the range of decreasing area (2–10N) the catalytic activity has already reached its maximum [30,31] and the *n*-butane conversion decreases. Moreover the only feature that correlates with the increase of catalytic activity is the increase in the sulfur surface density. The increase in sulfur density until a value close to the half monolayer value is reached. The slight increase in the catalytic activity would make the pattern similar to that of the zone (2) in the curve of the aged catalyst. However zone (2) for the non-aged catalyst occurs with little variation of the specific surface area while in the case of the aged catalyst there exists a drastic decrease.

The results of activity as a function of time-on-stream for the *n*-butane reaction as obtained in the pulse reactor were plotted in Fig. 9. The activity of the non-aged gel was much higher than any of the aged and sulfated gels at all values of time-on-stream (pulse number). Selectivity values for two of the catalysts were included in Table 2. A monotonic decrease in activity was found for all catalysts. Selectivity to *i*-butane increased with time-on-stream as it is commonly found on these catalysts indicating that strong acid sites needed for skeletal branching are deactivated by coke deposition.

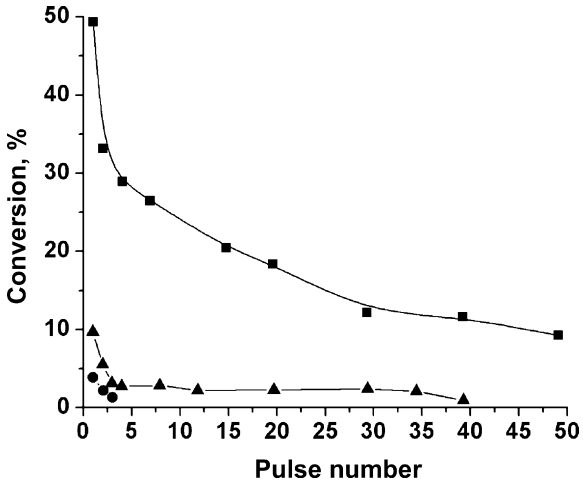

Fig. 9. Activity as a function of time-on-stream (pulse number *n*-butane) for different sulfate promoted zirconia catalysts. (■) Non-aged aged zirconia gel sulfated with 1N SO_4H_2; (■) aged zirconia gel sulfated with 9N SO_4H_2; (●) aged zirconia gel sulfated with 1N SO_4H_2.

The selectivity values of Table 2 correspond to the first and fifth pulse. For the latter, the conversion rate had dropped to almost one half. Selectivity to C_1–C_3 was taken as a measure of the extent of cracking reactions. Selective to cracking products was important in the first pulse but it decreased with time-on-stream. In the fifth pulse the selectivity to C_1–C_3 was low and the selectivity to *i*-C_4 and C_5 increased. Cracking reactions were less important in the case of the reflux aged catalyst SZ^{AG} and the selectivity to *i*-C_4 was higher.

The results of the reaction of isomerization-cracking of *n*-octane are included in Table 3. This reaction is known to have less demanding requirements regarding the acid strength of the active sites. Isomerization-cracking of *n*-octane has been routinely taken as a model test reaction for the hydrocracking of long paraffinic cuts. From the point of view of the upgrading of long paraffins into gasoline range fuels the objective is to maximize the liquid yield and to increase the selectivity to branched isomers. Among the liquid products preferred compounds are multibranched high RON compounds while among the light gases the most valuable is isobutane. As it can be seen in Table 3 both catalysts deactivate as

Table 3
n-Octane reaction

	Catalyst			
	Pt/SZ^{AG}		Pt/SZ	
	30 min[a]	240 min[a]	30 min[a]	240 min[a]
Conversion (%)	6.16	4.64	18.50	14.31
Yield C_1 (%)	–	–	–	–
Yield C_{2-3} (%)	0.40	0.30	0.44	0.58
Yield *n*-C_4 (%)	0.90	0.52	0.44	0.08
Yield *i*-C_4 (%)	1.22	0.73	0.37	0.22
Liquid yield, C_{5-8} (%)	3.22	3.09	17.25	13.31
Yield *i*-C_{5-8} (%)	2.99	2.89	16.68	12.38
Selectivity *i*-C_{5-8} (%)	48.46	62.39	90.14	93.00

Activity and yields to different products as two values of time-on-stream. Catalysts imprenated with 1N H_2SO_4 and calcined at 600 °C.
[a] Time (min).

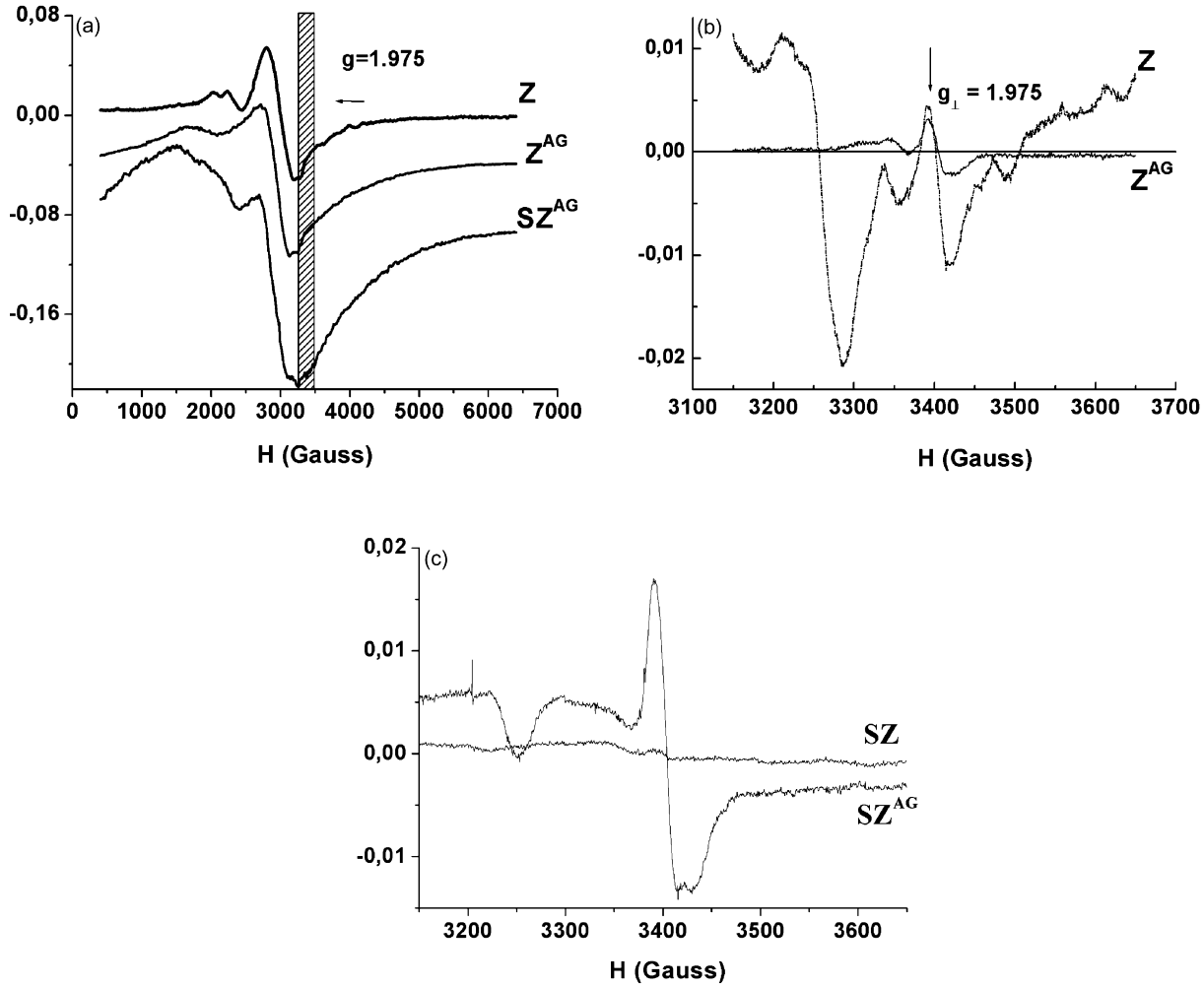

Fig. 10. ESR spectra of aged and non-aged samples. (a) Samples dried at 100 °C; (b) sulfur-free samples calcined at 600 °C; (c) sulfated samples calcined at 600 °C. Shaded bar: region where Zr^{3+} signals are detected in the calcined samples.

reflected by the decrease in conversion at 240 min from the initial value at 30 min. At 240 min time-on-stream a pseudo steady state was reached. Inspection of the initial or the final stable values reveal the same differences between the aged and the non-aged catalysts. The total conversion for the aged catalyst was much lower. Both catalysts displayed a null hydrogenolysis activity (no methane was produced) and this was attributed to the interaction of Pt with the support, an extensively reported effect for Pt supported over sulfated zirconia. The aged catalyst had an important cracking activity with isobutane as main cracking-isomerization product. The liquid yield on SZ^{AG} was also very low and this was correlated both to the low conversion and to the high cracking selectivity. These results can be explained by recalling that the distribution of acid sites is displaced in the case of the aged catalyst to the formation of strong acid sites. In the case of the non-aged catalyst most acid sites had mild acid strength. This catalyst displayed the best performance values. Especially important were the liquid yield and the yield to branched C_{5-8} isomers which were four times higher than those of SZ^{AG}.

3.1.5. Assessment of surface defects by ESR and NO adsorption

Aging of the gel before sulfation was clearly negative for the catalytic performance of the catalysts in spite of the textural properties being greatly improved. The results of catalytic activity can not be explained by simple models relying on regular acid sites because the activity in *n*-butane isomerization was not correlated to surface area, sulfur content, sulfur density, total acidity or concentration of strong acid sites. An alternative explanation would be that isomerization sites in sulfated zirconia are mostly related to "irregular" sites rather than to Zr cations or sulfate groups on regular zirconia planes, specially in the case of the active sites needed for isomerization of *n*-butane. This hypothesis has been some times formulated in the early studies of sulfated zirconia catalysts. Based on IR data Yamaguchi proposed that Lewis acid sites of sulfated zirconia were responsible for the activation of alkane at low temperature. The importance of the coordinative unsaturated sites was also illustrated, indicating that the active sites were developed at the edge or corner of the metal oxide surface [36]. Vera et al. [37] postulated that oxygen vacancies in sulfated zirconia catalysts could play a role in stabilizing the charge of carbeniums and hence play an important role in active catalysts.

In line to the previous reasoning aging is known to remove gel defects and hence produces crystalline materials with fewer imperfections after calcination. For example the aging of alumina has been shown to eliminate the presence of abnormal penta-coordinated aluminum in sulfated alumina catalysts [38]. The presence of a more regular surface in the aged gels was indirectly demonstrated in our results by the nitrogen adsorption tests, with dried Z^{AG} samples having a much lower BET constant than the Z sample. Additional ESR and FTIR tests were performed in order to

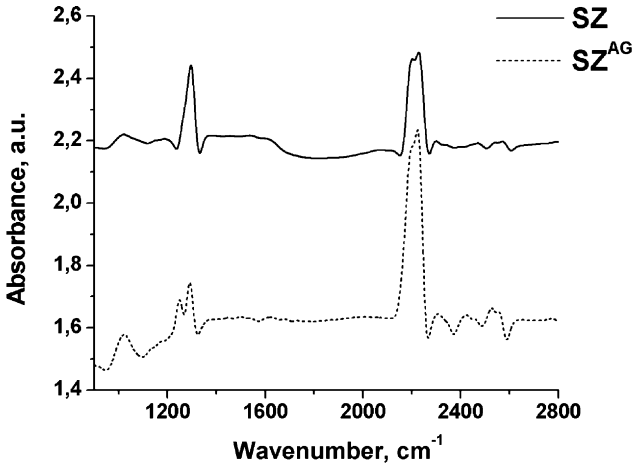

Fig. 11. FT-IR spectra of NO adsorbed on the SZ and SZ^{AG} samples calcined at 600 °C.

see if surface imperfections were indeed eliminated by hydrothermal aging leading to the disappearance of some active sites in the final catalysts.

Fig. 10 contains the relevant ESR spectra. ESR tests were made in order to check the presence of Zr^{3+} species. Previous works by other authors [39] on polycrystalline samples have associated Zr^{3+} to a narrow and anisotropic line with g-factor values: $g\perp = 1.975$ and $g// = 1.957$. These Zr^{3+} species are usually associated to the presence of oxygen vacancy defects, because the remaining electrons left by the oxygen lost are shared by nearby Zr cations and paramagnetic Zr^{3+} centers are formed. The spectra in Fig. 10a correspond to the uncalcined gels and indicate that the samples are highly paramagnetic. However no Zr^{3+} signals can be found in these samples. The concentration of paramagnetic species is higher in the aged sample.

The ESR spectra of the calcined samples are included in Fig. 10b and c. In these spectra signals due to Zr^{3+} are found at $g = 1.975$. In the case of the unsulfated samples hydrothermal aging and calcination produce samples that have approximately one half the concentration of Zr^{3+} species in comparison to non-aged samples. In the case of the sulfated samples the trend is drastically reversed. The SZ sample calcined at 600 °C had the lowest concentration of Zr^{3+} species. Its spectrum showed practically no signals of paramagnetic species. SZ^{AG} has a much higher concentration of Zr^{3+}. This concentration is also higher than that of the corresponding Z^{AG} sample with no sulfate. These ESR data do not help to elucidate the real role of anionic vacancies, if any, because there is no clear correlation between the concentration of Zr^{3+} species and the catalytic activity observed. Also notice that in materials with low electrical conductivity, and consequently high skin depth, as it is the case with ZrO_2, the sample bulk and surface, both, contribute to the observed ESR absorption.

The results of FTIR absorption of adsorbed NO can be found in Fig. 11. Only the relevant region of the spectrum where absorption occurred is plotted. Bands of adsorbed N_2O can be found at 2243 and 1226 cm^{-1}. These bands appear both in the sulfated and unsulfated samples (not shown). These bands are commonly attributed to the ν(N–N) and ν(N–O) vibration modes of adsorbed N_2O [40]. The 2ν(N–O) overtone is located at 2450 cm^{-1} and could not be detected in the tested simples. The ν(N–O) and 2ν(N–O) are located at lower frequencies in the sulfate free simples (1233 cm^{-1} and 2466 cm^{-1}) and this is due to the higher acidity of the sulfated samples [40].

A band at about 1900 cm^{-1} corresponding to a $Zr^{+4}(NO_3^-)$-NO surface species [40] could not be found in the recorded spectra. This band usually appears in the spectrum of ZrO_2 when O_2 is present in the adsorption cell. A weak negative band at 1380–1390 cm^{-1} was found in the case of the sulfated simples that coincides with previous reports of N_2O species adsorbed on adjacent sulfate groups [41]. This band would be typical of the sulfate group and would be shifted to lower frequencies upon interaction with the adsorbate.

No bands due to the oxidation of NO to NO_2 were detected. The bands associated to NO reduction were those found at 2300–2100 cm^{-1} and were associated to the absorbance of NO^+ centers that donate π electrons to surface cations. The bands at 1226 cm^{-1} are a particular case of generic bands of N species on transition metal oxide cations partially oxidized by NO, which are routinely found at frequencies lower than 1700 cm^{-1}.

Integration of the absorption bands at 1226 cm^{-1} and 2200 cm^{-1} indicates that the ratio of the areas $(SZ^{AG}/SZ)^{1126} \approx 1$ and $(SZ^{AG}/SZ)^{2200} = 2.17$. A higher concentration of surface oxygen abducting sites, i.e. of sites that reduce NO to N_2O, is displayed by the Z^{AG}. This is in contrast with a supposition that oxygen vacancies and coordinatively unsaturated cations are less abundant on the hydrothermally aged materials.

Based on the ESR and the NO adsorption data the hypotheses of a possible relation between the concentration of anionic vacancies and activity in isomerization should be disregarded. The remaining most likely reason for the results found could be that based on the works of Yamaguchi [36] and Morterra et al. [35] that indicate that on freshly precipitated zirconia gels, sites related to edges, corners and kinks in crystallographic planes are the first to be sulfated and convert into stable and very active sites upon calcinations. The removal of these sites by hydrothermal aging could be the cause for the observed drastic decrease in activity. Further experimental work is needed to confirm this hypothesis.

4. Conclusions

Reflux aging greatly improved the textural properties of oxoanion promoted zirconia catalysts. The available surface area, sintering resistance and tetragonal/monoclinic ratio were higher than those of non-aged materials. Particularly the specific surface area of hydrothermally aged sulfated zirconia was 220 $m^2\ g^{-1}$ after calcination at 600 °C. Stabilization of the tetragonal structure was practically complete in the whole technical temperature range of use of the catalysts and was likely related to a surface energy effect.

The activity pattern of hydrothermally aged sulfated zirconia was unusual. Aging was clearly negative to the catalytic activity, specially in *n*-butane isomerization. For this reaction low values of conversion were got under all conditions of sulfation and a monotonic increase of conversion with sulfuric acid concentration was found in spite of a continuous drastic decrease of the surface area.

Both the *n*-butane and *n*-octane reactions proceeded with low conversion on the hydrothermally aged catalyst. In the case of the *n*-octane reaction not only the conversion was lower but also the activity to cracking products was higher. The increased cracking activity was correlated with the higher concentration of strong acid sites on the aged catalyst. The lower activity in isomerization of *n*-butane was attributed to a loss of sites of medium acid strength, specifically those related to sulfate on crystal defects removed by the aging procedure.

References

[1] B.H. Davis, R.A. Keogh, R. Srinivasan, Catal. Today 20 (1994) 219.
[2] X. Song, A. Sayari, Catal. Rev. Sci. Eng. 38 (1996) 329.
[3] J.M. Parera, Catal. Today 15 (1992) 481.
[4] R.A. Comelli, C.R. Vera, J.M. Parera, J. Catal. 151 (1995) 96.
[5] J.C. Yori, C.R. Vera, J.M. Parera, Appl. Catal. A 163 (1997) 165.

[6] F.R. Chen, G. Coudurier, J.F. Joly, J.C. Vedrine, J. Catal. 143 (1993) 616.
[7] S. Chokkaram, B.H. Davis, J. Mol. Catal. A: Chem. 118 (1997) 89.
[8] D.A. Ward, E.I. Ko, J. Catal. 150 (1994) 18.
[9] D.A. Ward, E.I. Ko, J. Catal. 157 (1995) 321.
[10] R.A. Boyse, E.I. Ko, J. Catal. 171 (1997) 191.
[11] S.J. Reddy, A. Sayari, Catal. Lett. 38 (1996) 219.
[12] P. Liu, J.S. Reddy, A. Adnot, A. Sayari, In: R.F. Lobo, J.S. Beck, S.L. Suib, D.R. Corbin, M.E. Davis, L.E. Iton, S.I. Zones (Eds.), Materials Research Society Symposium Proceedings, vol. 431, 1996, p. 101.
[13] G.N. Sauvion, Demande de Brevet d'invention, FR (1985) 2 590 887-A1.
[14] R. Franklin, P. Goulding, J. Haviland, R.W. Joyner, I. Mc Alpine, P. Moles, C. Norman, T. Nowell, Catal. Today 10 (1991) 405.
[15] R.A. Boyse, E.I. Ko, J. Catal. 179 (1998) 100.
[16] A.L. Costa Pereira, S.G. Marchetti, A. Albornoz, P. Reyes, M. Oportus, M. do Carmo Rangel, Appl. Catal. A 233 (2008) 187.
[17] F.C. Jentoft, A. Hahn, J. Kröhnert, G. Lorenz, R.E. Jentoft, T. Ressler, U. Wild, R. Schlögl, C. Häßner, K. Köhler, J. Catal. 224 (2004) 124.
[18] H.E. Bergna, Ullmann's Encyclopedia of Industrial Chemistry, fifth ed., VCH, Weinheim, 1993.
[19] P. Afanasiev, C. Geantet, M. Lacroix, M. Breysse, J. Catal. 162 (1996) 143.
[20] G.K. Chua, S. Jaenicke, S.A. Cheong, K.S. Chan, Appl. Catal. A 145 (1996) 267.
[21] J.E. Huheey, Inorganic Chemistry, in: Principles of Structures and Reactivity, third ed., Harper & Row Publishers, New York, 1983.
[22] C. Morterra, G. Cerrato, C. Emanuel, V. Bolis, J. Catal. 142 (1993) 349.
[23] C.R. Vera, J.M. Parera, J. Catal. 165 (1997) 254.
[24] M.T. Tran, N.S. Gnep, G. Szabo, M. Guisnet, Appl. Catal. A 207 (1998) 171.
[25] C.G. Kontoyannis, G. Carountzos, J. Am. Ceram. Soc. 77 (1994) 2191.
[26] C.M. Phillippi, K.S. Mazdiyasni, J. Am. Ceram. Soc. 54 (1971) 254.
[27] S.R. Vaudagna, R.A. Comelli, N.S. Fígoli, Appl. Catal. A 164 (1997) 265.
[28] G. Štefanić, S. Musić, K. Molčanov, J. Alloys Compd. 387 (2005) 300.
[29] J. Yu, G. Wang, B. Cheng, M. Zhou, Appl. Catal. B: Environ. 69 (2007) 171.
[30] M. D'Amato, G. Costa, C.R. Vera, J.M. Parera, A. Escribano, R. Brizzi, Actas VII Jornadas Argentinas Catálisis, Mar del Plata, Argentina, September 1991, vol. I, p. 131.
[31] K. Mukaida, T. Miyoshi, T. Satoh, In: K. Tanabe, H. Hattori, T. Yamaguchi, T. Tanaka (Eds.), Acid-Base Catalysis, Proceedings of the International Symposium on Acid-Base Catalysis, Tokyo, 1988, p. 363.
[32] T. Yamaguchi, K. Tanabe, Mater. Chem. Phys. 16 (1986) 67.
[33] R. Silver, C.J. Hou, J.G. Ekerdt, J. Catal. 118 (1989) 400.
[34] J.C. Yori, J.M. Parera, Appl. Catal. A L151 (1995) 129.
[35] C. Morterra, G. Cerrato, S. Di Ciero, M. Signoretto, A. Minesso, F. Pinna, G. Strukul, Catal. Lett. 49 (1997) 25.
[36] T. Yamaguchi, Appl. Catal. 61 (1990) 1.
[37] C.R. Vera, C.L. Pieck, K. Shimizu, J.M. Parera, Appl. Catal. A 230 (2002) 137.
[38] M.L. Guzmán-Castillo, E. López-Salinas, J.J. Fripiat, J. Sánchez-Valente, F. Hernández-Beltrán, A. Rodríguez-Hernández, J. Navarrete-Bolaños, J. Catal. 220 (2003) 317.
[39] W. Khaodee, B. Jongsomjit, P. Praserthdam, S. Goto, S. Assabumrungrat, J. Mol. Catal. A: Chem. 280 (2008) 35.
[40] K. Hadjiivanov, V. Avreyska, D. Klissurski, T.S. Marinova, Langmuir 18 (2002) 1619.
[41] B. Tsyntsarski, V. Avreyska, H. Kolev, T.S. Marinova, D. Klissurski, K. Hadjiivanov, J. Mol. Catal. A 193 (2003) 139.